Effects of Confinement in Carbon Nanotubes on the Activity, Selectivity, and Lifetime of Fischer−Tropsch Co/Carbon Nanotube Catalysts

Ahmad Tavasoli,[†] Mariane Trépanier,[‡] Ajay K. Dalai,*[,‡] and Nicolas Abatzoglou[§]

School of Chemistry, University College of Science, University of Tehran, Tehran, Iran, Department of Chemical Engineering, University of Saskatchewan, Saskatoon, SK, S7N5C5 Canada, and Department of Chemical Engineering, Université de Sherbrooke, Sherbrooke, QC, J1K 2R1 Canada

The effects of electronic properties of the inner and outer surfaces of carbon nanotubes (CNTs) on the deactivation of cobalt Fischer−Tropsch (FT) catalysts were studied. The comparative characterization of the fresh and used 0.20 *w* (mass fraction) Co/CNT catalysts by transmission electron microscopy (TEM), X-ray diffraction (XRD), temperature-programmed reduction (TPR), Brunnauer−Emmett−Teller analysis (BET), and H_2 chemisorption showed that cobalt reoxidation, cobalt-support interactions, and sintering are the main sources of catalyst deactivation. TEM showed that continuous FT synthesis for 480 h increased the average Co particle size located inside the pores from (7 to 8.5) nm, while the average Co particle size located outside of the tubes increased from (11.5 to 25) nm. XRD analysis of the used catalyst confirmed cobalt reoxidation, interaction between cobalt and CNTs, and the creation of carbide phases. At a high percent CO (%CO) conversion and H_2O partial pressure, the deactivation rate is zero-order and independent of the number of active catalyst sites. In this case, the main deactivation mechanisms are cobalt reoxidation and metal support interactions. At lower %CO conversion and H_2O partial pressure, the deactivation rate can be simulated with power law expressions of the order of 11.4 for the particles outside the tubes and 30.2 for the particles inside the tubes. In this case, the main deactivation mechanism is sintering. Because of the electron deficiency of the inner sides of the CNTs, the interaction between the cobalt oxides and the support is stronger, leading to lower rates of sintering as compared with the particles located on the outer layers of the CNTs. Regeneration recovered the catalyst activity with 9.1 % of the total activity loss.

1. Introduction

Fischer−Tropsch synthesis (FTS) is a promising option for the environmentally friendly industrial production of chemicals and fuels from biomass, coal, and natural gas where a high-performance catalyst plays an essential role.[1,2] In the FTS process, the catalyst activity, selectivity, and lifetime are influenced by the nature and structure of support, nature of metal phase, metal dispersion, metal loading, and catalyst preparation method.[3,4] Cobalt catalysts are believed to deactivate less rapidly and yield higher linear alkanes than iron counterparts due to high chain growth probability. Thus, cobalt catalysts are considered to be the best candidates for syngas to clean liquid fuel requirements.[1] Most studies on cobalt FTS catalysts have been carried out with the metals supported on silica, alumina, or titania. Other families of supports with carbonaceous bases such as activated carbon have also been investigated for FT reactions.[5−13] As a FTS catalyst support, activated carbon has many advantages including resistance to acidic or basic media and stability at high temperatures. Carbon nanotubes (CNTs) possess similar properties and outperform activated carbon in most cases.[13] The unique properties of CNTs such as uniform pore size distribution, meso- and macropore structure, inert surface properties, and resistance to acid and base environments can play an important role in many catalytic reactions.[13] In our previous work we have reported interesting catalytic properties of CNT-supported cobalt catalysts prepared by the sequential aqueous incipient wetness impregnation method.[5−9] From a catalytic activity standpoint, the FT synthesis rate and percent CO (%CO) conversion obtained by CNT-supported cobalt catalysts were (40 to 45) % higher than that obtained with alumina-supported cobalt catalysts with the same cobalt loading in both fixed bed and slurry reactors.[6,7] CNTs also caused a slight decrease in the FTS product distribution to lower molecular weight hydrocarbons, requiring a smaller hydrocracker in the product upgrading section.[8]

Co/CNT-catalyzed FT synthesis is advantageous in carbon utilization as compared to processes using Co/Al_2O_3, Co/SiO_2, or Co/TiO_2 catalysts, but CNT-supported cobalt catalysts are more expensive necessitating a longer catalyst lifetime.[5−9] Therefore, catalyst stability is an important performance variable in the Co/CNT-catalyzed FT process. In the case of silica, alumina, and titania-supported cobalt catalysts, the potential causes of cobalt FTS catalyst deactivation includes (a) oxidation of the cobalt surface, (b) cobalt support interactions and formation of mixed compounds that are reducible only at high reduction temperatures, (c) sintering, (d) refractory coke formation, (e) loss of metal cobalt because of attrition, and (f) heteroatoms poisoning (i.e., sulfur).[14−16]

The present work investigates the deactivation properties of CNT-supported cobalt catalysts during continuous FT synthesis for 480 h in a fixed-bed microreactor, considering different deactivation mechanisms. The main objective of this work is

* Corresponding author. E-mail: ajay.dalai@usask.ca. Phone: (306)-966-4771. Fax: (306)-966-4777.
[†] University College of Science.
[‡] University of Saskatchewan.
[§] Université de Sherbrooke.

10.1021/je900984c
Published on Web 04/13/2010

to study the effect of electronic properties of the inner and outer surfaces of the CNTs on the deactivation of Co/CNT catalysts.

2. Experimental Section

2.1. Catalyst Preparation. Purified multi-wall carbon nanotubes (MWCNT) were used as support material for the preparation of the FTS catalyst. Prior to impregnation, the support was treated with 0.30 *w* (mass fraction) HNO_3 at 100 °C overnight, washed with distilled water, and dried at 120 °C for 6 h. The purified CNTs were loaded with 0.20 *w* cobalt using sequential incipient wetness impregnation of cobalt nitrate solution ($Co(NO_3)_2 \cdot 6H_2O$ 99.0 %, Merck). After each impregnation step, the catalyst was dried at 120 °C for 6 h and calcined at 350 °C for 3 h at a heating rate of 10 °C·min^{-1} under argon flow. The cobalt loadings of the calcined fresh and used catalysts were verified by an inductively coupled plasma atomic emission spectroscopy (ICP-AES) system.

2.2. Transmission Electron Microscopy (TEM). Morphology of the support and the fresh and used catalysts was studied by transmission electron microscopy (TEM). Sample specimens for the TEM studies were prepared by ultrasonic dispersion of the catalysts in ethanol and the suspensions dropped onto a copper grid. TEM investigations were carried out using a Hitachi H-7500 (120 kV). Several TEM micrographs were recorded for each sample and analyzed to determine the particle size distribution.

2.3. BET Surface Area Measurements and Pore Size Distributions. The surface area, pore volume, and average pore radius of the support and the fresh and used catalysts were measured by an ASAP-2010 system from Micromeritics. The samples were degassed at 200 °C for 4 h under 50 mTorr vacuum, and their Brunnauer−Emmett−Teller (BET) area, pore volume, and average pore radius were determined.

2.4. X-ray Diffraction. X-ray diffraction (XRD) measurements of the support and the fresh and used catalysts were conducted with a Philips PW1840 X-ray diffractometer with monochromatized Cu/Kα radiation. Using the Scherrer equation, the average size of the cobalt oxide crystallites in the calcined fresh and used catalysts were estimated from the line broadening of the cobalt oxide peaks.

2.5. Temperature-Programmed Reduction. Temperature-programmed reduction (TPR) spectra of the fresh and used catalysts were recorded using a Micromeritics TPD-TPR 290 system, equipped with a thermal conductivity detector. To remove traces of water, the catalyst samples were first purged in a flow of argon at 100 °C and then cooled to 40 °C. The TPR of 50 mg of each sample was performed using 5.1 % hydrogen in argon gas mixture with a flow rate of 40 cm^3·min^{-1}. The samples were heated from (40 to 800) °C with a heating rate of 10 °C·min^{-1}.

2.6. Hydrogen Chemisorption. The amount of chemisorbed hydrogen on the fresh and used catalysts was measured using the Micromeritics TPD-TPR 290 system. 0.25 g of the sample was reduced under hydrogen flow at 400 °C for 12 h and then cooled to 100 °C under hydrogen flow. To remove the weakly adsorbed hydrogen, the flow of hydrogen was then switched to argon at the same temperature, for about 30 min. The temperature-programmed desorption (TPD) of the samples was obtained by increasing the temperature of the samples to 400 °C with a ramp rate of 20 °C·min^{-1} under argon flow. The TPD spectrum was used to determine the cobalt dispersion and its surface average crystallite size using the following equations.[15,16]

$$\text{calibration value } (l_{gas}/\text{area units}) = \frac{\text{loop volume} \times \%\ \text{analytical gas}}{\text{mean calibration area} \times 100} \quad (1)$$

$$\text{H}_2\ \text{uptake (moles/g}_{cat}) = \frac{\text{analytical area from TPD} \times \text{calibration value}}{\text{sample weight} \times 24.5} \quad (2)$$

$$\%D_{\text{TotalCo}} = \frac{\text{H}_2\ \text{uptake} \times \text{atomic weight} \times \text{stoichiometry}}{\%\ \text{metal}} = \frac{\text{number of Co}^{\text{o}}\ \text{atoms on the surface} \times 100}{\text{total number of Co}^{\text{o}}\ \text{atom}} \quad (3)$$

$$\%D_{\text{reducedCo}} = \frac{\text{number of Co}^{\text{o}}\ \text{atoms on the surface} \times 100}{\text{total number of Co}^{\text{o}}\ \text{atom} \times \text{fraction reduced}} \quad (4)$$

$$\text{diameter (nm)}_{\text{totalCo}} = \frac{6000}{\text{density} \times \text{maximum area} \times \text{dispersion}} \quad (5)$$

$$\text{diameter (nm)}_{\text{reducedCo}} = \frac{6000}{\text{density} \cdot \text{maximum area} \times \text{dispersion} \times \text{fraction reduced}} \quad (6)$$

2.7. Reaction Setup and Experimental Outline. The catalyst was evaluated in terms of FTS activity ($g_{HCproduced} \cdot g_{cat}^{-1} \cdot h^{-1}$) and selectivity (the percentage of the converted CO that appears as hydrocarbon products) in a fixed-bed microreactor. The reactor temperature was controlled via a PID temperature controller. Brooks 5850 mass flow controllers were used to add H_2, CO, and argon at the desired rate to the reactor. Argon was used as an internal standard gas in the reactor feed. Prior to the activity tests, the catalyst activation was conducted according to the following procedure: The catalyst (1 g) was placed in the reactor, and pure hydrogen was introduced at a flow rate of 60 mL·min^{-1}. The reactor temperature was increased from room temperature to 380 °C at a rate of 10 °C·min^{-1} and maintained at this activation condition for 20 h, and the catalyst was reduced in situ. After the activation period, the reactor temperature was decreased to 180 °C under flowing hydrogen.

The synthesis gases entered through the top of the fixed-bed reactor at a flow rate of 52.4 mL·min^{-1} (H_2/CO ratio of 2). The reactor pressure was increased to 2 MPa, and the temperature was increased to 220 °C at a rate of 10 °C·min^{-1}. Products were continuously removed from the vapor and passed through two traps, one maintained at 100 °C (hot trap) and the other at 0 °C (cold trap). The uncondensed vapor stream was reduced to atmospheric pressure through a back-pressure regulator. The composition of the outlet gas stream was determined using an online GC-2014 Shimadzu gas chromatograph. Contents of the hot and cold traps were removed every 24 h and analyzed by a Varian 3400 GC liquid chromatograph.

After 480 h of the first FT synthesis step, the flow of synthesis gas was switched off, and the catalyst was rereduced (second treatment step) in a flow rate of 60 mL·min^{-1} H_2 at 270 °C for 20 h. The second FT synthesis step was carried out under the same conditions and the activity ($g_{HCproduced} \cdot g_{cat}^{-1} \cdot min^{-1}$) and selectivity of the system measured. The third treatment step of the catalyst was performed at 380 °C for 20 h, cooled to 220 °C, and carried out under the same conditions as the previous synthesis steps. The products were analyzed under the same conditions as the first synthesis step. The catalytic bed was

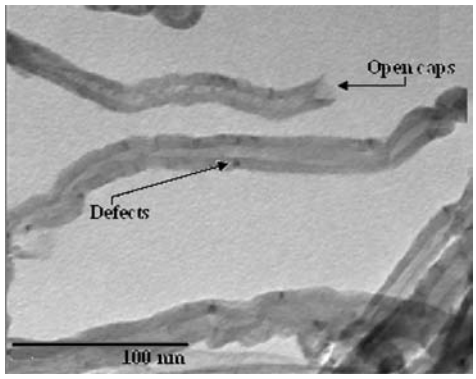

Figure 1. TEM image of the CNTs as support material after acid treatment.

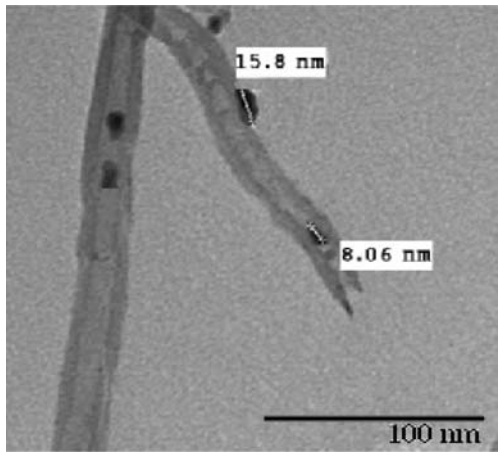

Figure 2. TEM image of the calcined fresh catalyst.

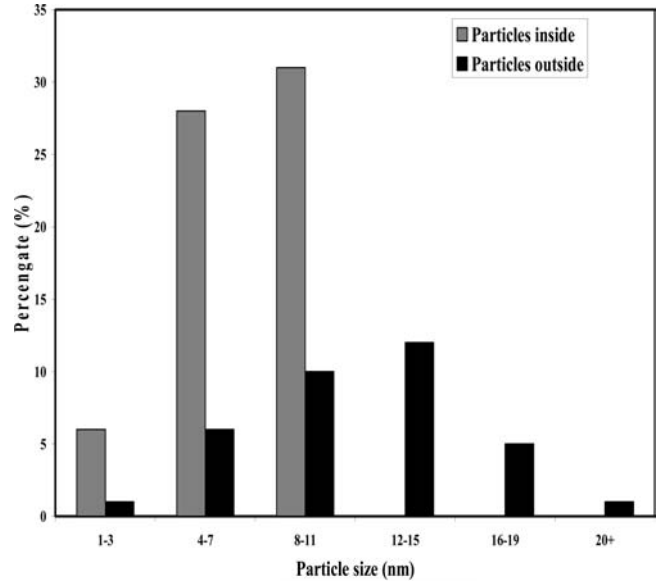

Figure 3. Cobalt oxide particle size distribution of calcined fresh cobalt oxide on CNT catalyst.

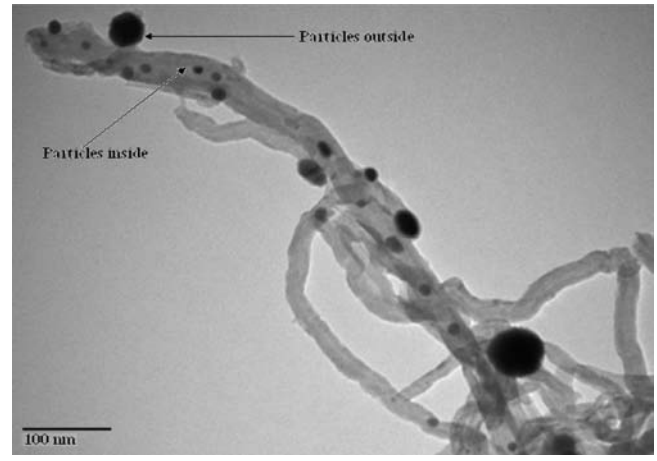

Figure 4. TEM image of the used catalyst.

treated by helium flow for 3 h at 270 °C to remove the heavy waxes inside the catalyst pores. The temperature of the reactor was lowered to 20 °C, and the catalyst was passivated with pulses of dry air to stop further oxidation. The used catalyst was discharged and characterized extensively.

3. Results and Discussion

3.1. Characterization Overview. A sample of the purified CNT material was analyzed by TEM. The purified product consisted of an interwoven matrix of tubes (Figure 1) comprised of multiwalled CNTs. The TEM image of calcined fresh catalyst revealed that the catalyst particles were well-dispersed inside the tubes and also on the perimeter of the tube walls (Figure 2). Dark spots represent the cobalt oxides which are attached either inside or outside the nanotubes. This figure shows that the majority of the cobalt particles, about (65 to 70) %, are distributed in the inner pores of the CNTs. This can be attributed to the tubular morphology of CNTs that can induce capillary forces during the impregnation process. The particle sizes were calculated using the following equation $d = (4ab/\pi)^{0.5}$ where a and b are the dimensions of the particles as seen in the TEM image. In the fresh catalyst, the size of the cobalt oxide particles located inside the CNTs are fairly uniform with the most abundant in the range of (4 to 11) nm, which is accordance with the average inner diameter of the CNTs (12 nm). The cobalt oxide particles located on the outer surface have grown to about 16 nm (Figure 2). Clearly, the CNT channels restricted particle growth inside the tubes. A bar graph depicting the size distribution of the total particle populations inside and outside the tubes for the calcined catalyst is shown in Figure 3. This figure shows that the average particle size of the particles located on the inner surface of the tubes is about 7 nm and that of the particles located on the outer surface of the tubes is about 11.5 nm.

Figure 4 shows a TEM picture of the used catalyst, which shows that particles inside the CNTs are still small [(4 to 11) nm] while the particles attached to the outer surfaces of the CNTs have grown significantly (i.e., > 40 nm). There is no significant cobalt oxide agglomeration inside the CNT channels, a phenomenon related to both the interaction of the metal site with the inner surface of the tubes and to the spatial restriction of the CNT channels. However, on the exterior surface most of the cobalt oxides agglomerated, resulting in lower metal site dispersion under FT reactions. The tubular morphology of the grapheme layers make CNTs different compared to other carbonaceous supports. The studies by Chen et al. reveal that the deviation of the grapheme layers from planarity causes the π-electron density to shift from the concave inner surface to the convex outer surface, leading to an interior electron-deficient surface and an exterior electron-enriched surface.[17−19] This characteristic can influence the structure and electronic properties of metals in contact with either surface of the CNTs. It can be concluded that, due to the electron deficiency of the inner sides of the CNTs, the interaction between the cobalt oxides and the support could be stronger, thus leading to lower rates of sintering

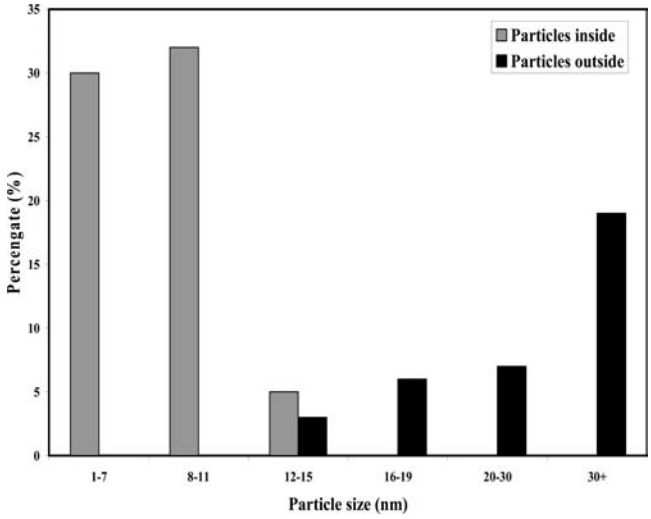

Figure 5. Cobalt oxide particle size distribution of the used catalyst.

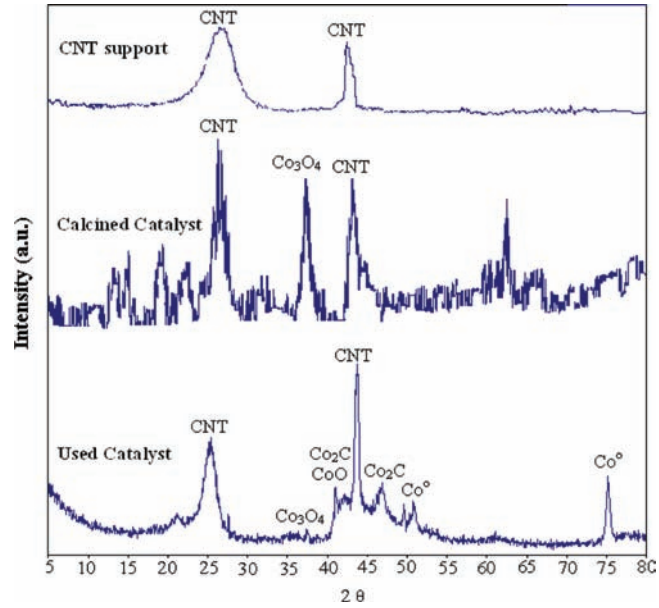

Figure 6. XRD spectra for the pure CNTs, fresh and used 0.20 *w* Co/CNT catalysts.

than that of the particles located on the outer layer of the CNTs. Furthermore, since the particles inside the tubes are rather less mobile, the sintering occurrence is considerably limited.

A bar graph depicting the size distribution of the total cobalt oxide particle populations inside and outside the tubes for the used catalyst is presented in Figure 5. Comparing Figures 3 and 5 clearly shows that the sintering rate of the particles located on the outer surface of the CNTs is more significant than for particles on their inner surface. In the case of the particles located on the inner surface of the tubes, the average particles size increased from (7 to 8.5) nm, and that of the particles located on the outer surface of the tubes increased from (11.5 to 25) nm.

Table 1 shows the metal contents for both the fresh calcined and the used catalysts. ICP analyses of the catalysts revealed that the metal contents of the catalysts was similar and close to the targeted metal content of 0.20 *w* Co. Table 1 also shows the results of the BET surface area measurements of the purified CNTs, fresh and used catalysts. In the case of the fresh calcined catalyst, a loading of 0.20 *w* Co decreased the surface area from (210 to 163) $m^2 \cdot g^{-1}$ and the pore volume from (0.6 to 0.47) $cm^3 \cdot g^{-1}$, indicating pore blockage due to cobalt loading on the support. After 480 h of FT synthesis, the catalyst BET surface area and the pore volume were further decreased from (163 to 121) $m^2 \cdot g^{-1}$ and from (0.47 to 0.36) $cm^3 \cdot g^{-1}$, respectively. Sintering of the particles and pore blockage during the FT synthesis causes a decrease in BET surface area and pore volume.

Figure 6 shows the XRD profiles of the purified CNTs and the fresh and used catalysts. The peaks at 2θ of 25° and 43° correspond to graphite layers (multiwall CNTs), while the other peak in the spectrum of the fresh catalyst (36.8°) relates to the crystal planes of Co_3O_4.[16] No peak was observed indicating formation of cobalt-support compounds in the fresh catalyst XRD spectrum. For the used catalyst, the peaks for CNT remain at a 2θ value of 25° and 43°. The peak at 42.5° in the XRD spectrum clearly indicates the presence of CoO compounds.[20,21] Co_3O_4 compounds were also observed in the spectrum of the used catalyst, but with a smaller peak than for the fresh catalyst at 36.8°. The metallic cobalt structure (Co°) is observed from the XRD pattern of the used catalyst at 51.5°.[16,20] Furthermore, the peak at a 2θ value of 47° correlates well with the Co_2C species.[16] Peaks for Co_2C may also be present at 36.8° and 45.7°, but these peaks are hidden in the broad peak of Co_3O_4 and CNT. The presence of Co_2C can be attributed to either cobalt CNT interaction or a Co/carbon reaction during the CO dissociative adsorption. Although a fraction of the cobalt clusters may oxidize in the presence of significant amounts of water formed during FT synthesis with high conversions, it is probable that a fraction of cobalt oxide is formed during the discharge and passivation step at room temperature. Table 1 shows the average cobalt oxide particle size of the fresh and used catalysts calculated from the XRD spectra and the Scherrer equation. In agreement with the results of the TEM analyses, XRD results show that there is a significant particle growth in the course of the FTS reaction. On the basis of the XRD profiles and the TEM studies, there is good agreement between the data for the average particle size calculated.

The activation of the fresh and used catalysts in a hydrogen atmosphere was proven by TPR experiments (Figure 7). The low temperature peak at (300 to 400) °C is typically assigned to the reduction of Co_3O_4 to CoO, although a fraction of the peak may be due to the reduction of the larger, bulk-like CoO species to Co°.[6,21] The second broad peak at (400 to 500) °C is assigned to the reduction of small CoO to Co° species and includes the reduction of cobalt species that interact with the support. The small peak at about 600 °C in is assigned to the gasification of the CNT.[8] For the used catalyst, the peaks shifted to lower temperatures, indicating that the reduction of the cobalt oxides occurred at lower temperatures than for the fresh calcined

Table 1. BET Surface Area, Porosity, XRD, and TPR Data for the Fresh and Used Catalysts

catalysts/support	ICP	BET $m^2 \cdot g^{-1}$	pore volume $cm^3 \cdot g^{-1}$	pore radius nm	XRD *d* nm	1st TPR peak °C	2nd TPR peak °C
CNT		210	0.6	6.1			
fresh catalyst	19.8	163	0.47	5.8	8.5	330	428
used catalyst	19.7	121	0.36	5.9	17	270	380

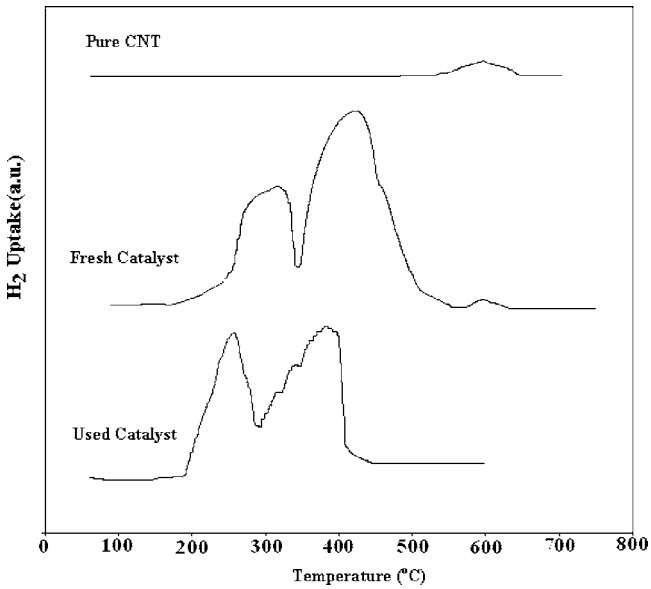

Figure 7. TPR profile for the pure CNTs, calcined fresh and used 0.20 *w* Co/CNT catalysts.

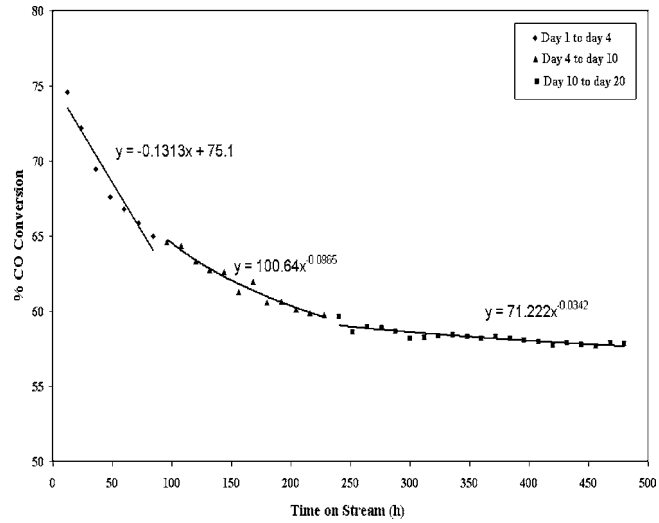

Figure 8. %CO conversion with time on stream ($T = 220$ °C, $P = 2$ MPa, $H_2/CO = 2$).

catalyst (Figure 7). According to Table 1, 480 h of FT synthesis decreased the first TPR temperature peak from (330 to 270) °C and the second TPR peak from (428 to 380) °C, suggesting an easier reduction process. A low reduction temperature can be due to either an easier reduction of larger cobalt particles (TEM and XRD) or to the presence of less stable oxides (XRD). However, in the case of the used catalyst the total H_2 consumption is lower, indicating a decrease in catalyst porosity due to particle growth and differentiation of the cobalt species (i.e., carbides). Therefore, it has been shown that the interaction of the metal oxide nanoparticles with the inner and outer CNT surfaces can affect the reduction behavior of the metal oxides.[17,18] The electron deficiency of the interior CNT surface can facilitate the reduction of the metal oxides located in the inner surface of the tubes as compared with the particles located in the outer surface of the tubes.[17,18] Sintering of the particles attached to the outer surface of the tubes during FT synthesis (as confirmed by TEM pictures) increased the ratio of the number of particles located inside the tubes to the number of particles located on the outer surface. In fact the ratio of the easily reducible particles to the total particles increased in the course of the FT reaction which could be another reason for the lower TPR peak temperature of the used calcined catalyst.

Results of H_2 chemisorption for the fresh and used catalysts are shown in Table 2. The data show that the hydrogen consumption for the used catalyst is lower than that of the fresh calcined catalyst. The percentage of reduction and dispersion calculated based on the total cobalt were decreased by about 10 %. The reduced cobalt also decreased significantly. In agreement with the TEM and XRD data, the particle diameters calculated on the basis of both the total cobalt and the reduced cobalt increased significantly with time on stream.

3.2. Fischer−Tropsch Synthesis. Table 3 presents the FT synthesis rate ($g_{CH}\cdot g^{-1}_{cat}\cdot h^{-1}$), % CO conversion, chain growth probability, and different product selectivities during first 12 h of FT synthesis. The FT synthesis productivity (0.4192 $g_{CH}\cdot g^{-1}_{cat}\cdot h^{-1}$) of the 0.20 *w* Co/CNT catalyst is greater than that of the commercial Al_2O_3, SiO_2, and TiO_2-supported cobalt-based FT synthesis catalysts.[6,22,15] However, its product distribution (13.7 % CH_4, 5.4 % C_2-C_4, and 79.7 % C_{5+} selectivity) shows a shift to the lower molecular weight hydrocarbons. It is to note that the FT synthesis rate of the commercial Al_2O_3, SiO_2, and TiO_2 supported cobalt catalysts are (0.25 to 0.32) $g_{CH}\cdot g^{-1}_{cat}\cdot h^{-1}$, and the CH_4 and C_{5+} selectivities are (4 to 6) % and (86 to 93) %, respectively.[22]

Figure 8 presents the CO conversion changes with time on stream of FT synthesis with 0.20 *w* Co/CNT catalyst. Three different deactivation steps are clearly distinguishable (1) during the first 4 days, the %CO conversion drops by 10 %, (2) during days 5 to 10, the %CO conversion drops by 4.7 %, and (3) during days 11 to 20, the %CO conversion drops by only 0.73 % and reaches a plateau region. The loss of active sites significantly decreases during the first 240 h of continuous FT synthesis. As Figure 8 shows, the profiles of declining curves of the first, second, and third step deactivations are different. For the first step, the deactivation curve is steeply sloped, then is moderated for the second step, and slowly levels off for the final step. The loss of activity for the first deactivation step can be simulated with the following linear correlation:

$$X_{CO} = -0.13T_{hr} + 75.1 \qquad (7)$$

The linear deactivation mode suggests that the order of the deactivation rate to %CO conversion is zero. This reveals that

Table 2. Percentage Dispersion and Crystallite Sizes of Unreduced and Reduced Cobalt Particles in 0.20 *w* Co/CNT Catalyst Determined by H_2 TPR

catalyst	$\mu mol_{H_2 desorbed}\cdot g_{cat}^{-1}$	% red.	% dispersion (tot. Co)	% dispersion (red. Co)	dp/nm (tot. Co)	dp/nm (red. Co)
fresh catalyst	221.4	63.9	10.4	16.3	9.9	6.3
used catalyst	178.9	53.4	8.4	15.7	17.5	9.4

Table 3. FT Synthesis Results for 12 h (220 °C, 2 MPa, $H_2/CO = 2$, GSHV = 3000 h^{-1})

% CO conversion	FT synthesis rate $g_{HC}\cdot g^{-1}_{cat}\cdot h^{-1}$	α	CO_2 selectivity	CH_4 selectivity	C_2-C_4 selectivity	C_{5+} selectivity
74.6	0.4192	0.86	1.2	13.7	5.4	79.7

during the first four days, the FTS deactivation rate is independent of the number of catalyst active sites and that deactivation is caused by exterior factors.[14,22,23] It has been suggested that in FT synthesis on cobalt-based catalysts at high conversions, the loss of activity is caused by water-induced oxidation of cobalt.[14−16,20,22] This deactivation process entails cobalt redox transformation with no support participation. Another reason for this type of activity loss is the formation of more refractory forms of oxidized cobalt generated by cobalt-support interactions.[20,22] The extent of this type of deactivation also depends on the partial pressure of water produced during FT synthesis. It was recommended that water promotes interaction between cobalt oxide species and support.[15,16] Thus, the larger deactivation observed during the first 4 days of FT synthesis can be due to higher partial pressure of water as an exterior factor present in the catalytic bed of the reactor.[14−16,20,22] In other words, a CNT-supported cobalt catalyst is more susceptible to reoxidation and cobalt-support interactions at higher water partial pressures. Thermodynamic studies on the stability of nanosized metallic cobalt crystallites in water/syngas mixtures show that, under realistic FTS conditions the oxidation of bulk metallic cobalt is not feasible, unless the water partial pressure relative to the hydrogen and carbon monoxide partial pressures is in excess of (50 to 60) %.[24,26] However, the oxidation of small cobalt crystallites to Co(II)O or the formation of an oxide shell might be thermodynamically feasible under specific conditions. The stability of nanosized crystallites, which are related to dispersion of cobalt particles, is dependent on the ratio of surface energy to the overall system energy that may vary with crystallite size, morphology, the starting crystal phase, and the ratio of the partial pressure of water relative to the partial pressure of the syngas. It is shown that spherical cobalt crystallites with a diameter less than 4.4 nm are not stable, thus leading to higher catalyst deactivation under industrial FT conditions.[9,20,23] The decrease in %CO conversion during the first 4 days may come from the oxidation of these nanosized cobalt crystallites.

For the second and third deactivation steps, the catalyst deactivation could be simulated with the following power law expressions:

$$\text{second step: } X_{CO} = 100.64 T_{hr}^{-0.0965} \quad (8)$$

$$\text{third step: } X_{CO} = 71.22 T_{hr}^{-0.0342} \quad (9)$$

Assuming the deactivation rate is:

$$-\frac{dX}{dt} = kX^n \quad (10)$$

After integration and data reduction by least-squares, the power order (n) can be determined as 11.4 and 30.2 for the second and the third deactivation steps, respectively. These values are in the range that ordinary metal catalysts would experience during sintering.[23] The low n value (11.4) for the second deactivation step demonstrates that the rate of sintering during this step was significantly higher than that for the third step. The TEM test results showed that the rate of sintering of the particles located on the outer surfaces of the CNT is higher than that of the particles located on the inside of the tubes. The zone with the higher sintering rate (Figure 8, step 2) can be attributed to the sintering of the particles located in the outer layers of the tubes, and the zone with the lower sintering rate (Figure 8, step 3) can be attributed to the sintering of the particles located inside the tubes. The results of H_2 chemisorptions and reoxidation tests shown in Table 2 confirm the cluster growth during the 480 h reaction. A FT synthesis temperature of 220 °C is low to enhance the cluster growth at the catalyst surface, but the water vapor increases the oxidation−reduction cycles on the catalyst surface that in turn leads to cluster growth or sintering. These results verify that, to have a Co/CNT catalyst with a longer lifetime, it is necessary to distribute the active metal particles in the inner layers of the CNTs. Introducing functional groups and defects on the CNT surfaces can also act as anchoring sites for the cobalt particles and hence decrease sintering rate of the cobalt particles which are located on the outer layer of the CNTs.[8]

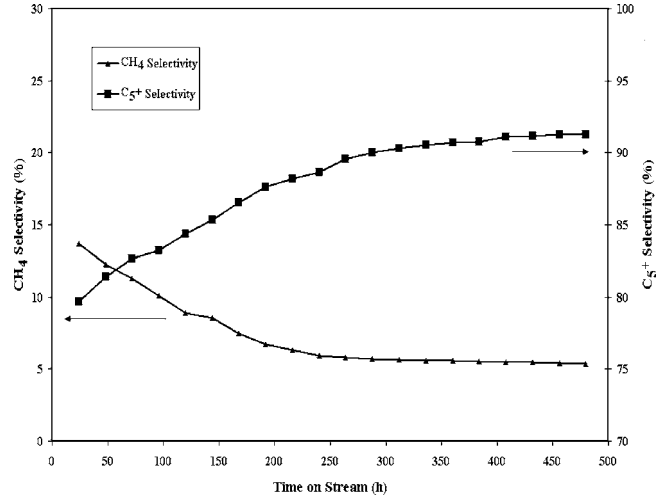

Figure 9. Products selectivity with time on stream (T = 220 °C, P = 2 MPa, H_2/CO = 2).

The regeneration of the used catalyst at (270 and 380) °C increased %CO conversion from (57.9 to 63.5) % and from (63.5 to 67.1) %, respectively. The total activity recovery after the third regeneration step at 380 °C (about 9.1 %) is close to the total activity loss during the first deactivation step (about 10 %). Since the catalyst deactivation due to sintering is an irreversible process, the activity recovery can be assigned to the reduction of reoxidized cobalt and the reduction of cobalt species that interacted with the support (step 1).

The uncondensed vapor stream of the cold trap was reduced to atmospheric pressure through a pressure letdown valve, and the composition of this stream was quantified using an online gas chromatograph. The contents in the hot and cold traps were removed every 24 h. The hydrocarbon and water fractions were separated and analyzed using a Varian CP 3400 GC. Figure 9 shows the methane and C_5^+ liquid hydrocarbon selectivity variations with time on stream. This figure displays that, during 480 h FT synthesis at 220 °C and 2 MPa, CH_4 selectivity decreases and C_{5+} selectivity increases with time on stream. The studies of Bezemer et al. have shown that the larger cobalt particles are more selective to higher molecular weight hydrocarbons and smaller ones are selective to methane and light gaseous hydrocarbons.[9,25] It can be concluded that sintering of the smaller particles leads to enhancement of C_{5+} selectivity and suppression of CH_4 production with time on stream.

As discussed earlier, most of the cobalt particles are located inside the CNTs. Confinement of the reaction intermediates inside the pores can enhance their contact with cobalt particles, favoring the growth of longer chain hydrocarbons. In addition, the inner sides of the CNTs are electron-deficient and can enhance the dissociation of CO resulting in the production of higher hydrocarbons chain. Increasing the ratio of the particles located inside the tubes to the particles located outside the tubes

is believed to be the main reason for enhancement of C_{5+} selectivity and suppression of CH_4.

4. Conclusions

Cobalt catalysts supported on CNTs have shown two different types of deactivation mechanisms: cobalt oxidation and sintering. Sintering is the main source of irreversible deactivation in the CNT-supported cobalt FT synthesis catalysts. The deposition of cobalt particles inside the CNT pores improves the catalytic behavior of the Co/CNT catalyst, which is likely due to the difference in the electronic properties of the inner and outer surface of the CNTs and cobalt particle confinement effects. Because of the electron deficiency of the inner sides of the CNTs, the interaction between the cobalt oxides and the support is stronger, leading to lower rates of sintering as compared with the particles located on the outer layers. Also, the physical encapsulation of the metal particles inside the pores reduces the metal site sintering. Confinement of reaction intermediates inside the channels increases the contact time with active metal sites, resulting in the production of heavier hydrocarbons.

Abbreviations

FTS	Fischer−Tropsch synthesis
TOS	Time on stream
BET	Brunauer, Emmett, and Teller
CNTs	Carbon nanotubes
XRD	X-ray diffraction
TPR	Temperature-programmed reduction
ICP	Inductively coupled plasma
TEM	Transition electron microscopy
SEM	Scanning election microscopy
TPD	Temperature-programmed desorption

Nomenclature

P	Pressure (MPa)
T	Temperature (°C)
%CO	Percent of CO conversion (by mol %)

Literature Cited

(1) Michiel, J. A.; Tijmensen, M. J. A.; Faaij, A. P. C.; Hamelinck, C. N.; Van Hardeveld, M. R. M. Exploration of the possibilities for production of Fischer−Tropsch liquids and power via bimass gasification. *Biomass Bioenergy* **2002**, *23*, 129–152.

(2) Dry, M. E. Fischer−Tropsch reactions and the environment. *Appl. Catal., A* **1999**, *189*, 185–190.

(3) Zhang, J.; Chen, J.; Ren, J.; Li, Y.; Sun, Y. Support effect of Co/Al_2O_3 catalysts for FTS. *Fuel* **2003**, *82*, 581–586.

(4) Bukur, D. B.; Lang, X.; Mukesh, D.; Zimmerman, W. H.; Rosynek, M. P.; Li, C. Binder/support effects on the activity and selectivity of iron catalysts in Fischer−Tropsch synthesis. *Ind. Eng. Chem. Res.* **1990**, *29*, 1588–1599.

(5) Tavasoli, A.; Rashidi, A.; Sadaghiani Zadeh, M.; Karimi, A.; Kodadadi, A.; Mortazavi, A. European Patent EP1782885, 2005.

(6) Tavasoli, A.; Sadagiania, K.; Khorasheb, F. A. A.; Seifkordib, A.; Rohani, A.; Nakhaeipoura, A. Cobalt supported on carbon nanotubes − A promising novel Fischer−Tropsch synthesis catalyst. *Fuel Process. Technol.* **2008**, *89*, 491–498.

(7) Tavasoli, A.; Malek Abbaslou, R. M.; Trépanier, M.; Dalai, A. Fischer−Tropsch synthesis over cobalt supported on carbon nanotubes in a slurry reactor. *Appl. Catal., A* **2008**, *345*, 134–142.

(8) Trépanier, M.; Tavasoli, A.; Dalai, A. K.; Abatzoglou, N. Fischer−Tropsch synthesis over carbon nanotubes supported cobalt catalysts in a fixed bed reactor. *Fuel Process. Technol.* **2009**, *90*, 367–374.

(9) Bezemer, G. L.; Bitter, J. H.; Kuipers, H. P. C. E.; Oosterbeek, H.; Holewijn, J. E.; Xu, X.; Kaptejin, F.; Jos Van Dillen, A.; de Jong, K. P. Cobalt Particle size Effects in the Fischer−Tropsch Reaction studied with Carbon Nanofiber Supported Catalysts. *J. Am. Chem. Soc.* **2006**, *128*, 3956–3964.

(10) Ma, W.; Kugler, E. L.; Wright, J.; Dadyburjor, D. B. Mo-Fe catalysts supported on Activated Carbon for synthesis of liquid fuels by the Fischer−Tropsch Synthesis process: Effect of Mo addition on reducibility, activity, and hydrocarbon selectivity. *Energy Fuels* **2006**, *20*, 2299–2307.

(11) Ǧuczi, L.; Stefler, G.; Geszti, O.; Koppány, Z.; Kónya, Z.; Molnár, É.; Urbánc, M. I.; Kiricsi, J. CO hydrogenation over cobalt and iron catalysts supported over multiwall carbon nanotubes: Effect of preparation. *J. Catal.* **2006**, *244*, 24–32.

(12) van Steen, E.; Prinsloo, F. F. Comparison of preparation methods of carbon nanotubes supported iron FTS. *Catal. Today* **2002**, *71*, 327–334.

(13) Serp, P.; Corrias, M.; Kalck, P. Carbon nanotubes and nanofibers in catalysis. *Appl. Catal., A* **2003**, *253*, 337–358.

(14) Tavasoli, A.; Nakhaeipour, A.; Sadaghiani, K. Cobalt supported on carbon nanotubes Apromising novel Fischer−Tropsch synthesis catalyst. *Fuel Process. Technol.* **2007**, *88*, 461–468.

(15) Jacobs, G.; Patterson, P. M.; Das, T.; Luo, M.; Davis, B. Fischer−Tropsch synthesis: Effect of water on Co/Al_2O_3 catalysts and XAFS characterization of reoxidation phenomena. *Appl. Catal., A* **2004**, *270*, 65–76.

(16) Jacobs, G.; Das, T. K.; Zhang, Y.; Li, J.; Racoillet, G.; Davis, B. H. Fischer−Tropsch synthesis: support, loading, and promoter effects on the reducibility of cobalt catalysts. *Appl. Catal., A* **2002**, *233*, 263–281.

(17) Chen, W.; Fan, Z.; Pan, X.; Bao, X. Effect of Confinement in Carbon Nanotubes on the Activity of Fischer−Tropsch Iron Catalyst. *J. Am. Chem. Soc.* **2008**, *130*, 9414.

(18) Pan, X.; Fan, Z.; Chen, W.; Ding, Y.; Luo, H.; Bao, X. Enhanced ethanol production inside carbon-nanotube reactors containing catalytic particles. *Nat. Mater.* **2007**, *6*, 507–511.

(19) Menon, M.; Andriotis, A. N.; Froudakis, G. E. Contrasting bonding behaviors of 3*d* transition metal atoms with graphite and C_{60}. *Phys. Lett.* **2000**, *320*, 425–431.

(20) Tavasoli, A.; Malek Abbaslou, R. M.; Dalai, A. Deactivation behavior of ruthenium promoted Co/γ-Al_2O_3 in Fischer−Tropsch synthesis. *Appl. Catal., A* **2008**, *346*, 58–64.

(21) Trépanier, M.; Tavasoli, A.; Dalai, A. K.; Abatzoglou, N. Co, Ru and K loadings effects on the activity and selectivity of carbons nanotubes supported cobalt catalyst in FTS. *Appl. Catal., A* **2009**, *353*, 193.

(22) Tavasoli, A.; Irani, M.; Malek Abbaslou, R. M.; Trépanier, M.; Dalai, A. K. Morphology and deactivation behaviour of Co-Ru/Al_2O_3 Fischer−Tropsch synthesis. *Can. J. Chem. Eng.* **2008**, *86*, 1070–1080.

(23) Bartholomew, C. H. Mechanism of catalyst deactivation. *Appl. Catal., A* **2001**, *212*, 17–60.

(24) van Steen, E.; Claeys, M.; Dry, M. E.; van de Loosdrecht, J.; Viljoen, E. L.; Visagie, J. L. Stability of nanocrystals: thermodynamic analysis of oxidation and re-reduction of cobalt in water/hydrogen mixtures. *J. Phys. Chem. B* **2005**, *109*, 3575–3577.

(25) Tavasoli, A.; Sadaghiani, K.; Nakhaeipour, A.; Ahangari, M. G. Raising distillate selectivity and catalyst lifetime in Fischer−Tropsch synthesis by using a novel dual-bed reactor Iranian. *J. Chem. Eng.* **2007**, *26* (1), 1–9.

(26) Kiss, G.; Kliewer, C. E.; DeMartin, G. J.; Culross, C. C.; Baumgartner, J. E. Hydrothermal deactivation of silica-supported cobalt catalyst in Fischer−Tropsch synthesis. *J. Catal.* **2003**, *217*, 127–140.

Received for review November 19, 2009. Accepted March 14, 2010.

JE900984C